



Final Technical Report

**College of Letters,
Arts and Sciences**

Department of
Earth Sciences

Submitted to the

**United States Geological Survey
Reston, VA 20192**

**Site Effects and Seismic Properties of the San Andreas Fault
Zone Using the Varian Vertical Array, Parkfield, California**

USGS Grant 1434-95-G-2559

**PI: Rachel Abercrombie
Department of Earth Sciences
University of Southern California
Los Angeles, California 90089-0740**

October, 1998

University of
Southern California
Los Angeles
California 90089-0740
Tel: 213 740 6106
Fax: 213 740 8801

Crustal Attenuation and Site Effects at Parkfield, California

Rachel E. Abercrombie

Department of Earth and Planetary Sciences, Harvard University,

Manuscript in Preparation for submission to Journal of Geophysical Research

13 October, 1998

Please address correspondence to:

Dr. R. E. Abercrombie

Department of Earth and Planetary Sciences

Harvard University

20 Oxford Street

Cambridge MA 02138

Tel. 617 495 9604

Fax. 617 495 0635

email. Abercrombie@seismology.harvard.edu

Abstract

The recordings of 9 earthquakes in 10 boreholes (≤ 1000 m deep) and at 6 surface sites are combined to quantify the attenuation in the upper crust at Parkfield, California, where the San Andreas fault separates strongly contrasting rock types – high velocity Salinian granite to the SW and lower velocity Franciscan basement to the NE. I find that the attenuation on the NE side of the fault is approximately twice that on the SW side ($Q_{SW} \sim 2Q_{NE} \sim 200$) in the depth range about 200 m to 5 km. P and S wave spectral modeling, and also an inversion of spectral ratios between borehole recordings at different depths (in which the source is eliminated) both give consistent results. Varying the assumed velocities and earthquake locations affects the absolute Q values, but the ratio remains stable. Q_P and Q_S are similar, but their ratio is not well resolved. Recordings in the fault zone are combined with the inversion results to estimate $Q_P \sim 50$ and $Q_S \sim 80$ in the fault zone, confirming that it is a low Q , low velocity zone. Q is also observed to increase with depth, with the rate of increase decreasing as the depth increases. In the upper 1 km at the Varian Well, $Q_P \sim 30$ and $Q_S \sim 20$, with Q_P increasing from about 20 between 0 and 300 m to about 55 between 600 and 900 m. This study confirms that the borehole seismometers at Parkfield are not deep enough for the effects of attenuation to be ignored in analyses of small earthquakes. Also, interestingly, the attenuation below 1 km on the NE side of the fault is comparable to that below about 200 m on the SW side. Amplification and resonance effects are clearly seen in the shallowest layers, but the results of this study suggest that in calculating site effects, the very shallow layers (surficial geology, <30 m) and the attenuation at intermediate depths (a few hundred to a few thousand meters) are of comparable importance.

1. Introduction

The aim of this study is to measure attenuation in the upper crust at Parkfield, as a function of depth on each side of the San Andreas fault, and also within the fault zone. To do this, I combine earthquake recordings from two borehole networks, as well as using some surface seismometers, and build on the large body of previous work in this area.

Studies of near surface attenuation and amplification have become commonplace in seismic hazard analyses as the importance of these site effects in controlling strong ground shaking has been recognized (e. g. at Mexico City, *Celebi et al.*, 1987).

Knowledge of the site effects and attenuation in the upper few kilometers is also important in earthquake source analyses. For example, ambiguity between source, site and path effects caused *Archuleta et al.* [1982] to report an apparent breakdown in small earthquake scaling which has since been shown to result from severe near surface attenuation [*Abercrombie and Leary*, 1993; *Abercrombie* 1997]. Lack of constraints on attenuation at Parkfield have led to uncertainty in earthquake source parameters, even at shallow borehole stations [e. g. *Blakeslee and Malin*, 1991; *Johnson and McEvilly*, 1995]. Knowledge of attenuation is also important to characterizing the rock mass. For example, scattering attenuation can be used to investigate the fracture density (ref. 19?), and the attenuation within a fault zone may be an indicator of its mechanical behavior and rheology. Previous studies using pairs of earthquakes [*Blakeslee et al.*, 1989] and fault zone trapped waves [e. g. *Li et al.*, 1990] suggest that major faults are typically zones of low velocity and low Q .

Studies of attenuation in the crust using only surface seismometers have found Q to increase with depth, from quite low values near the surface [e. g. *Hough and Anderson*, 1988; *Scherbaum*, 1990]. This work is constrained by the relatively high noise levels at surface sites, and also because of the narrow frequency bandwidth available. The strong attenuation at shallow depths prevents high frequency signals from being recorded. Also,

there is an inherent ambiguity between the absolute value and the depth extent of the near surface low Q [Scherbaum, 1990].

The installation of borehole seismometers has greatly improved our knowledge of site effects and near surface attenuation. Borehole seismograms are typically lower noise and wider bandwidth than surface ones because high frequency energy is recorded which is attenuated before reaching surface instruments. Comparison of recordings at a few hundred meters depth and at the surface constrains Q to be about 10 in this depth range [e. g. *Blakeslee and Malin*, 1991; *Aster and Shearer*, 1991], and the amplification can also be measured. Deeper boreholes (1–3 km) show Q increasing with depth [e. g. *Hauksson et al.*, 1987; *Jongmans and Malin*, 1995; *Abercrombie*, 1997]. *Abercrombie* [1998] reviews the contribution of borehole recordings of earthquakes to our knowledge of attenuation, both in the near surface and at seismogenic depths.

An interesting question to consider is how deep must a seismometer be to be beneath the site effect. At Cajon Pass, where the deep instruments are over 2 km into granitic bedrock, this was sufficient for depth for the site effect to be ignored [*Abercrombie and Leary*, 1993; *Abercrombie*, 1995; 1997]. At other sites with thicker sedimentary sequences (for example the Los Angeles basin, *Hauksson et al.* 1987, or Parkfield) deeper installations may be necessary.

The region around Parkfield, on the San Andreas fault, central California, has been well instrumented and well studied on account of the Parkfield prediction experiment (ref 19??). The presence of a borehole network (averaging about 250 m depth) spanning the San Andreas fault, as well as instruments at a range of depths, to almost a kilometer, at the Varian well (see figure 1) allow any lateral variations and depth dependence of attenuation to be investigated without the severe limitations of surface data.

The Parkfield area is an interesting one to study because of the very different basement rocks juxtaposed by the San Andreas fault [*Page*, 1981; *Sims*, 1988; 1990]. To the south-

west (SW) of the fault is the Salinian block of, principally granitic, plutonic arc rocks. To the north-east (NE) of the San Andreas fault, the Franciscan assemblage, a melange of subduction related trench and oceanic sediments, with fragments of more resistant rock, forms the basement. On both sides of the fault, the basement rocks are covered by 1–2 km of Quaternary and Tertiary sediments. Two 3-D velocity inversions in the Parkfield area have both found significant differences across the fault, with the velocities to the SW averaging 0.5–0.75 km/s faster than to the NE at Middle Mountain [*Michellini and McEvilly*, 1991; *Eberhart-Phillips and Michael*, 1993]. *Eberhart-Phillips and Michael* [1993] show that the 3-D velocity structure agrees well with the basement geology of the region.

Although there have been no large earthquakes at Parkfield since 1966, there are abundant smaller events which are well recorded by the borehole networks. The earthquakes are thought to occur within the San Andreas fault zone and are highly clustered [e. g. *Nadeau et al.*, 1994]. The frequency content of the seismograms recorded on each side of the fault, and also at Middle Mountain within the fault zone, suggests that the lower velocity rocks on the NE side are probably more attenuating than those to the SW, and that the fault zone could be even lower Q [*Nadeau et al.*, 1994; *Johnson and McEvilly*, 1995]. Previous studies also show that Q increases with depth, from about 10 in the upper few hundred meters [*Blakeslee and Malin*, 1991; *Jongmans and Malin*, 1995] on both sides of the fault, and *Jongmans and Malin* [1995] put some constraints on S wave Q in the upper kilometer at the Varian well.

In the present study, I combine available borehole data, and some surface recordings to investigate shallow and crustal attenuation using a variety of spectral methods. First I model the borehole amplitude spectra, assuming a source function, to estimate the earthquake source parameters and attenuation on each side of the San Andreas fault. I also compare P and S wave recordings at different depths in the Varian well to measure Q as a function of depth in the upper kilometer. Then, I combine all the borehole recordings to invert for attenuation as a function of depth, on each side of the San Andreas fault. and

also within the fault zone. Finally, I compare the borehole recordings to those at nearby surface stations to estimate the shallow attenuation and site effects.

2. Data

In this study I use the recordings of nine earthquakes from three independent seismic networks in the Parkfield area. The earthquakes are those for which data were available from the Varian array, and are a subset of those used by *Jongmans and Malin* [1995]. I retain their event numbering. These earthquakes were originally selected on account of the high signal-to-noise ratio at the Varian array. They are also in the right magnitude range ($M_L 1 - 2.1$) to be well recorded by the HRSN.

These earthquakes are included in three independent seismicity catalogs: (a) the NCSN catalog (based on P wave arrival times from the USGS network with station corrections to align the earthquakes with the surface trace of the San Andreas fault), (b) The Duke University catalog which uses automatically picked P and S arrivals recorded by the HRSN, and a 1-D velocity model, and (c) The Berkeley catalog (HRSN) which uses hand picked P and S arrival times on the HRSN and the 3-D velocity model of *Michellini and McEvilly* [1991]. These event locations and all the stations used in the study are shown in figure 1. The NCSN and HRSN locations are included in Table 1, and the Duke University locations are given by *Jongmans and Malin* [1995]. *Nadeau and McEvilly* [1997] compare the three catalogs, and two others with improved location accuracy. Of the three catalogs considered here, they find that the HRSN has the best relative location accuracy and the NCSN the worst. The HRSN catalog should be the superior as it uses the best quality data and the most realistic velocity model. The high velocity gradients near the San Andreas fault mean that the absolute positions of the earthquakes in the direction normal to the fault are not as well constrained. I, therefore, use both the HRSN and NCSN locations in the following analyses to investigate the effect of location uncertainty on the results.

2.1 Varian Well

The Varian A1 well is located approximately 1.5 km NE of the San Andreas fault, and was instrumented with a variety of downhole sensors in 1987 to a depth of 1.5 km [Malin *et al.*, 1987]. Unfortunately the deepest instruments soon failed, and in this study I use the seven working, high-gain, 3-component seismometers at depths of 0, 23.5, 298, 572, 877, 907 and 938 m. I refer to these stations as V000, V023, V298, V572, V877, V907 and V938, respectively. The instruments are all 4.5 Hz geophones, recorded at a rate of 500 samples/second (see Jongmans and Malin, 1995, for further description of the instrumentation).

2.2 HRSN

The shallow borehole, High Resolution Seismic Network (HRSN, also known as the Downhole Digital Seismic Network) was completed in 1987 and consists of ten 3-component stations at depths between 63 and 572 m [Malin *et al.*, 1989]. The sampling rate is 500 samples/second. Details of the instrumentation are given by Karageorgi *et al.* [1992]. The deepest instrument (572 m) is in the Varian well, and is the same sensor recorded by the Varian array as station V572. The availability of a sensor being recorded by two independent systems allows me to check the consistency of the data and also to compare the quality of the different recording systems.

2.3 NCSN

The USGS operates a number of surface seismometers in the Parkfield area as part of the Northern California Seismic Network (NCSN). Here I select the five 3-component stations closest to stations of the HRSN so as to investigate site effects and attenuation in the uppermost few hundred meters. These stations are recorded at 100 samples/second.

3. Method

3.1 Spectral Analysis

The analysis in this study is performed entirely in the frequency domain. I therefore begin by calculating displacement P and S spectra, corrected for the relevant instrument response, from all the records for each earthquake. I use time windows of both 0.5 and 1 s to investigate the effect of window length. I prefer relatively short time windows, as at Cajon Pass [Abercrombie, 1997], because I am interested in the direct waves, and so wish to minimize the effect of reflected and scattered waves. Both these window lengths are long compared to the source durations of earthquakes with M_L 1-2 (< 0.1 s, Abercrombie, 1995). The windows start just before the P and S arrivals, to allow for a 5% cosine taper. I perform all parts of this study with spectra calculated from both the 0.5 and 1 s time windows. I find no significant differences between the results from these two window lengths at any point, and so in the following I simply quote the results from the 1 s windows. The P and S amplitude spectra are summed over all three components (figures 2 and 3). No smoothing is performed, and only the frequency range in which the signal is at least 3 times the noise level is used in the subsequent analysis. The noise spectra are calculated from windows immediately preceding, and of the same duration, as the P and S windows. The P wave noise window is therefore the pre-event background noise level and the S wave noise window includes the P wave coda, thus preventing such energy from contaminating the S wave analysis. Any clipped records are also excluded.

As mentioned previously, the 572 m sensor in the Varian well is recorded by both the Varian array (V572) and the HRSN (VAR). I therefore compare the amplitude spectra for several earthquakes recorded at these two stations. Within the frequency range where the signal-to-noise ratio is high, the spectra at the two stations are identical, as would be hoped. The background noise level at V572 is consistently about five times higher than that at VAR. The noise level is similar for all of the instruments in the Varian array, suggesting that it is mainly composed of electronic, rather than environmental, noise. The lower noise in the HRSN recording system is consistent with the fact that better quality amplifiers were used in this network (P. Malin, pers. comm. 1995). The higher noise level

$$\Omega(f) = \frac{\Omega_0 e^{-(\pi f t / Q)}}{\left[1 + \left(\frac{f}{f_c} \right)^n \right]^{1/\gamma}} \quad (1)$$

where Ω_0 is the long period amplitude, f is the frequency, f_c the corner frequency, t the travel time of the wave being considered, Q the frequency independent quality factor, n the high frequency fall off on a log-log plot, and γ is a constant. Following *Abercrombie* [1995], I assume that $n = 2$, and $\gamma = 2$ to obtain a sharper corner than the standard Brune model [*Brune*, 1970; *Boatwright*, 1980]. The assumption of frequency independent Q is considered reasonable based on the small frequency dependence of Q at high frequencies found in previous studies [*Adams and Abercrombie*, 1998; *Abercrombie*, 1998], and also on the linear nature of the majority of the spectral ratios calculated in the present study.

I model the spectra recorded at eight stations of the HRSN and also at the deepest sensor in the Varian array (V938). Including the surface NCSN stations in this analysis is not worthwhile because of their relatively narrow signal bandwidth and larger site effects.

In order to estimate the effect of attenuation on the source parameters obtained, I also model the spectra with a second version of equation (1) in which I assume that attenuation is negligible ($Q = \infty$) and so omit the exponential term, set $\gamma = 2$, and allow n to vary.

4.1 Source Parameters

I calculate the source parameters seismic moment (M_0), source dimension (radius, r) and stress drop ($\Delta\sigma$) from the spectrum models following *Brune* [1970], *Madariaga* [1976] and *Eshelby* [1957] respectively. I assume a density of 2800 kg/m^3 , P wave velocity (α) of 5500 m/s , and $\mu = 3 \times 10^{10} \text{ N/m}^2$. All S wave velocities (β), except those calculated from S travel times, are assumed to be $\alpha/\sqrt{3}$. I calculate the hypocentral distances for all 3 sets of locations, assuming straight ray paths. These values are in good agreement with those

The mean source parameters for each event from the 1 second windows of both P and S waves, using the HRSN locations and assuming $n = \gamma = 2$ are shown in Table 2. The parameters obtained from the different hypocenter locations are indistinguishable, within the errors. The source parameters are plotted in Figure 4, and are typical for events of this magnitude [Abercrombie, 1995]. *They are also in good agreement with those obtained from empirical Green's function analysis by Johnson etc. ??* The relationship between M_0 and M_L ($\text{Log}_{10}(M_0) = 1.0 M_L + 10.4$) is also consistent with previous studies at Parkfield and elsewhere [Malin *et al.*, 1989; Abercrombie, 1996].

4.3 Q from Spectral Modeling

The estimated mean Q values for both P (Q_P) and S (Q_S) waves at the different stations are shown in Table 3. Note that events 5, 8, 11 and 12 are not used to stations FRO, VCA and VAR because the short hypocentral distances lead to large uncertainties in the travel time. Unfortunately, this leaves only one reading each for Q_S at FRO and VCA, but several clear trends are still observable. The Q of paths to the three stations on the SW side of the fault (VCA, SMN and FRO) is significantly higher than that along the paths to the HRSN stations on the NE side. The path to MMN has very low Q , as would be expected for paths within a fault zone which is thought to be a low velocity, low Q zone [Li *et al.*, 1997]. The station RMN has the lowest Q values and is also the shallowest station. It is only about one third the depth of the others. The paths to this station sample shallower depths than to the other stations, and so the lower values are consistent with Q decreasing towards the surface. This has been observed at Parkfield previously [Jongmans and Malin, 1995] and is confirmed in the following section of the present study. The dramatic decrease in Q at shallow depths is also observed elsewhere in borehole studies [e. g. Abercrombie, 1997; 1998].

To compare the two sides of the fault, I calculate the average estimates of all values obtained at the three stations on the SW side, and the three HRSN stations on the NE side, excluding the shallow RMN (Table 3). The attenuation beneath about 200 m is approximately twice as high on the NE side as on the SW side of the fault. It is interesting

to note that Q_P and Q_S are similar, almost indistinguishable within errors. The attenuation of the S waves is still higher, however, because they travel more slowly. These results are in good agreement with the pulse width measurements made by *Johnson and McEvilly* [1995]. They find that the minimum pulse widths are larger and more scattered at stations on the NE side of the fault implying greater attenuation, than stations on the SW side.

Also included in Table 3 are the Q_P and Q_S values estimated by the same method, for paths to the deepest sensor in the Varian well (938 m). Q_P is higher than any other station on the NE side, but Q_S is similar to the values of the shallower stations. More interestingly, the Q values to V938 are lower than to stations on the SW side of the fault. These results suggest that just installing instruments deeper does not produce the lowest attenuation. Ray paths through the lower velocity Franciscan rocks in the upper few kilometers on the NE side of the fault are clearly more attenuating than through the Salinian basement to shallower depths on the SW side.

The Q values obtained from paths to all the borehole stations at Parkfield are considerably lower than those to a seismometer at a depth of 2.5 km in the Cajon Pass borehole in southern California. [*Abercrombie*, 1995]. This instrument was over twice as deep as the deepest Varian seismometer, and was also over 2 km into granitic bedrock [e. g. *Abercrombie*, 1997]. *Abercrombie* [1995] estimates $Q_P = Q_S = 1000$ for paths from local earthquakes to this site, and these high values are confirmed by the frequency dependent Q study of *Adams and Abercrombie* [1998]. *Abercrombie and Leary* [1993] and *Abercrombie* [1995] show that such low attenuation has a negligible effect on the source parameters estimated for local earthquakes recorded at the deep borehole site. The same is not true for the borehole stations at Parkfield. They are a great improvement on surface sites recording higher frequencies with lower background noise and showing little site amplification [e. g. *Blakeslee and Malin*, 1991]. A comparison of the source parameters calculated assuming negligible attenuation with those in Table 2, however, shows that if attenuation is ignored, the moments are underestimated by about a factor of

2, the dimensions are overestimated by about 10% for P waves, and almost 50% for S waves, and hence the stress drops are underestimated by a factor of about 2.5 for P waves and 4 for S waves. Just because an instrument is installed in a borehole, even to a depth of nearly a kilometer, attenuation effects at high frequencies cannot be ignored. *Ref. Peggy, eGf*

5. Spectral Ratios from Varian Array

I use the spectral ratios calculated for each earthquake between the recordings made at various depths in the Varian Well, and the deepest instrument (V907 for event 3, V938 for all the other earthquakes) to investigate attenuation as a function of depth. The calculation of the spectral ratio between a shallow or surface recordings and a deeper one is the most straightforward method of measuring the amplification and attenuation on the path in between. This method has become standard practice in recent years [e. g. *Hauksson et al.*, 1987; *Aster and Shearer*, 1991; *Blakeslee and Malin*, 1991; *Jongmans and Malin*, 1995; *Abercrombie*, 1997]. The underlying assumption is that the deeper recording can be considered on the ray path between the source and the upper receiver. If we also assume that the attenuation is exponential and is caused by a frequency independent Q [e. g., *Anderson and Hough*, 1984] then the spectral ratio ($R(f)$) should be a straight line on a log-linear plot, and the attenuation can be calculated from:

$$\ln(R(f)) = \ln(A) - \frac{\pi f \Delta t}{Q} \quad (2)$$

where A is the amplification, f is the frequency, and Δt is the travel time between the two receivers. This relationship and its underlying assumptions have been found to match observations well in previous studies in the Los Angeles Basin [*Hauksson et al.*, 1987], at Cajon Pass [*Abercrombie*, 1997] and also in the Varian Well ([*Jongmans and Malin*, 1995]. Figure 5 shows spectra and ratios between various levels for event 5. These ratios between the different borehole instruments appear linear, implying that equation (2) is a reasonable model of the shallow attenuation. Site resonances and very near surface amplification can dominate some recordings at surface sites, masking the attenuation

effect [e. g. *Abercrombie*, 1997; 1998]. Also, the resolution of the Q estimates improves with larger $\Delta t/Q$, and higher frequencies (most sensitive to attenuation) being included in the ratio. Estimates of Q over wide depth ranges are thus more reliable than over smaller ones [e. g. *Abercrombie* [1998], and ratios including a surface seismometer are typically less well resolved than those between two borehole instruments because of both the site amplification and the narrower signal bandwidth of most surface recordings.

5.2 0/938 m and 23.5/938 m

Over half of the ratios between the surface station (V000) and the deepest are dominated by amplification and resonance effects and so are not well modeled by (2). The average amplification at about 2 Hz is around three for both P and S waves. *Jongmans and Malin* [1995] obtain a similar result for S waves and show that this amplification is probably occurring in the upper 23 m. They also demonstrate that the peaks in the spectrum are consistent with resonances within the shallow velocity structure at that Varian Well. The ratios using V000 are very similar to those using V023 and so I combine them to obtain a more reliable estimate of attenuation in the upper kilometer at the Varian site. I find $Q_P = 33$, and $Q_S = 18$, each with 1 standard deviation being about 30% of the mean. Q is probably very low in the upper 23 m (studies elsewhere suggest less than 10) but because Δt is relatively small, the overall effect is within the scatter of the values. *Jongmans and Malin* [1995] attempt to model the ratios between 0 and 23 m, but are unable to obtain a Q for this reason.

5.3 298/938 m

The ratios between V298 and the deepest instruments are the best resolved, because Δt is not too small and a wider signal bandwidth is recorded at this depth. Using equation (2) I estimate $Q_P = 30$, and $Q_S = 31$ (1 standard deviation is about 25% of the mean) between 298 and 938 m depth.

5.4 572/938 m

Stations V572 and V938 are essentially too close to resolve an estimate of Q from the spectral ratios. I therefore, use the difference in the t^* values calculated in the spectral modeling at VAR and V938 to estimate Q in this depth interval. The values for S waves are very scattered but those for P waves suggest $Q_P = 55$ (1 standard deviation is 30%) between 572 and 938 m.

5.5 0/298 m

Combining the above results suggests that Q increases gradually with depth, as expected from studies elsewhere [e. g. *Abercrombie*, 1997], and also as observed for S waves by *Jongmans and Malin* [1995] at Varian. I can estimate the attenuation between 0 and 298 m by subtracting the attenuation (t^*) between 298 and 938 m from that measured over the whole borehole. In this way, I obtain $Q_P \sim 20$, and $Q_S \sim 10$, although within reasonable error estimates they could be the same.

5.6 Summary and Comparison with *Jongmans and Malin* [1995]

The estimates of Q obtained here are in good agreement with previous studies elsewhere. Q_P is larger than or equal to Q_S which has also been found in previous studies [e. g. *Abercrombie* [1997; 1998].

It is interesting to compare the estimates made here with those obtained from similar data at the same site by *Jongmans and Malin* [1995]. They consider only S waves, and use substantially larger time windows of 4 seconds. They calculate ratios between different depth intervals and estimate Q_S of 8-12 between 298 and 572 m, and $Q_S \sim 65$ between 572 and 938 m. These values are well within the errors of those in the present study. *Jongmans and Malin* [1995] also estimate Q_S between 0 and 298 m by comparing the direct arrival with the surface reflected wave in the 298 m recordings. They obtain $Q_S \sim 8$ between 0 and 298 m, in excellent agreement with the $Q_S \sim 10$ estimated in the present study by a different method. *Jongmans and Malin* [1995] also note that both the V572 and V298 instruments are in low velocity zones which will lead to increased scatter when applying equation (2) and a simple model of Q increasing with depth.

The estimate of $Q_S = 18$ in the upper kilometer obtained here is substantially different from the result of *Jongmans and Malin* [1995] ($Q_S \sim 37$) for the same depth range, despite the large errors (the formal 95% confidence limits do not overlap). This cannot be caused by combining the V000 and V023 recordings in the present study because separately these two depth intervals give similar values, just with larger scatter. The attenuation in the upper kilometer should be equal to the sum of the attenuation in the individual depth intervals. In this study, subtracting the attenuation between 298 and 938 m ($Q_S \sim 31$) from that estimated in the upper kilometer ($Q_S \sim 18$) gives a value of $Q_S \sim 10$ between the surface and 298 m. This last value is in excellent agreement with that of *Jongmans and Malin* [1995] for the same interval ($Q_S \sim 8$). A simple calculation, however, shows that using either value between 0 and 298 m results in more attenuation than is expected from the entire upper kilometer if $Q_S = 37$. This value for Q_S in the upper kilometer would, therefore, appear too high. It is significantly larger than values obtained elsewhere for similar depth ranges. For example, *Hauksson et al.* [1987] find $Q_S \sim 25$ between 420 and 1500 m depth in the Los Angeles Basin, and *Abercrombie* [1997] obtains $Q_S \sim 25$ between 300 and 1500 m at Cajon Pass. The estimates of $Q_P \sim 33$ and $Q_S \sim 18$ in the upper kilometer in the present study are more consistent with these results and the velocity structure at the Varian Well. The most likely reason for the anomalously high estimate made by *Jongmans and Malin* [1995] is their use of such long time windows. They note that these windows include various reflected phases and even fault zone trapped waves and so the simple model of equation (2) is probably not such a good approximation for these ratios. In the present study shorter windows are preferred in order to focus on the direct wave and minimize the contributions from scattered and reflected phases.

In summary I find that both Q_P and Q_S are low in the upper 300 m, gradually increasing with depth and that averaged over the upper kilometer, $Q_P \sim 33$ and $Q_S \sim 18$.

6. Inversion for Q on Each Side of Fault

The estimates of attenuation in Section 4 and Table 3 all involve assumptions about the shape of the source spectrum. A method of determining attenuation, independent of the source would clearly be preferable. I do this by extending the spectral ratio technique used in the previous section to the situation where the reference station is not on the ray path between the source and upper receiver. The method I use is essentially the reduced spectral ratio techniques outlined by *Sanders* [1993]. This technique has primarily been used to invert data from explosions sources for crustal P wave attenuation. For example, Clawson 19?? used a formal inversion to image a low Q_P in Yellowstone caldera.

I use the spectral ratios between the HRSN and V938 (V907 event 3) stations to remove the source, as described above. I then model the individual ratios using equation (2) to obtain $\Delta t^* = \Delta t / Q$, where Δt is the difference in travel times between the source and each station used in the ratio. Δt^* should be equal to the attenuation along the ray path from the earthquake to the HRSN station minus that from the earthquake to the reference station, V938.

I can ignore the effects of the source radiation pattern and geometrical spreading because they principally affect the absolute amplitude of the recordings. They should not affect the relative amplitude as a function of frequency which is all I use here to calculate Δt^* .

I then use these values of Δt^* for each event at each HRSN station to invert for Q on each side of the fault, and also with depth.

6.1 Inversion Set up (*better title..?*)

The 3-D velocity and geological structure at Parkfield can be approximated by two 1-D models, one on each side of the San Andreas fault (see section 4.2). The earthquakes all occur within the fault zone and so waves travel to the SW stations through one model and to the NE stations through the other. If I assume that the ray paths of earthquakes to station MMN travel within the fault zone, then I can also estimate attenuation within the

San Andreas fault. I consider this after obtaining a preferred inversion result for the two sides of the fault, and so station MMN is not used in the inversion.

The velocity structure at Parkfield is relatively well known [*Eberhart-Phillips and Michael, 1993; Michelini and McEvilly, 1991*] and so the 1-D velocity models which I use are fairly well constrained. I base them on the average structure within the vicinity of Middle Mountain, as the HRSN covers a relatively small area centered there. My preferred velocity model is shown in Figure 6(c). I try variations on this model but they have little effect on the inversion results. All the models extend to 2 km above sea level to eliminate any problems with the free surface during the ray tracing. Although the HRSN stations are at about 250 m depth (Table 3) they are all above sea level. The actual top of the model is unimportant because none of the ray paths considered travel above the HRSN stations. Representative station and surface elevations are included in figure 6(c).

I use a simple ray tracing code based on HYPO71 (Lee and Lahr??) to calculate the travel times to each station through the individual velocity layers. For stations VCA, FRO and SMN I use the SW 1-D model and for the other 6 stations I use the NE 1-D model. I perform separate inversions for P and S waves, and calculate S wave travel times by assuming $\beta = \alpha / \sqrt{3}$. I vary the velocity models by adding slower shallow layers, and by varying the layer thicknesses but with no significant effects on the results. I also perform the entire inversion procedure using both the NCSN and HRSN locations to investigate the effect of location uncertainty. I check the calculated travel times against those observed and find no significant or systematic differences, suggesting that the calculated arrival times are reasonable approximations, within the expected scatter.

My preferred model assumes a unknown Q on each side of the fault in the upper crust, above a fixed high Q half space (referred to as Q_{99}). I assume that $Q_{99} = 1000$ for both P and S waves, and that it extends from 5 km depth (all depths are relative to sea level). This value is based on a number of Q studies which all find high values of Q below a few

kilometers depth. For example, *Hough and Anderson* [1988] find $Q \geq 1000$ below 5 km depth at Anza, and *Abercrombie* [1997] and *Adams and Abercrombie* [1998] calculate Q to be approximately 1000 at Cajon Pass below 2.5 km, both in California. Varying the value of Q_{99} would have very little effect because it is so high, and also because only two earthquakes (3 and 10) are significantly deeper than 5 km, few ray paths spend much time in this layer. If we assume that Q increases with depth, as appears typical elsewhere [*Adams and Abercrombie*, 1998], then varying the depth of the top of the Q_{99} layer would effect the average values obtained in the shallower layers. It is therefore important to state the depth range over which Q is estimated, since it is the average value of a varying parameter. Within the inversion, decreasing the depth of the top of the Q_{99} will simply squeeze more attenuation into a smaller depth interval and lead to lower Q for a smaller, shallower depth range. I cannot resolve this ambiguity with the available data, and so fix the top of the Q_{99} layer at 5 km, consistent with Q profiles obtained elsewhere.

I use a simpler Q model than velocity model on account of the number of data available and their distribution. In the basic model shown in figure 6(c) I assume one unknown Q layer on each side of the fault (referred to as Q_1 on the NE side and Q_2 on the SW side) extending between the depth of the HRSN stations and 5 km. The velocity layers are chosen so that the top of the Q_{99} layer (and any additional Q layers) corresponds to the top of a velocity layer so that travel times in each layer can be easily calculated.

I then generate the following equations for each station - event pair, depending on which side of the fault the station is:

$$\text{SW:} \quad \Delta t^* = \frac{t_2}{Q_2} + \frac{t_{99}}{Q_{99}} - \left(\frac{tv_1}{Q_1} + \frac{tv_{99}}{Q_{99}} \right) \quad (3)$$

$$\text{NE:} \quad \Delta t^* = \frac{t_1}{Q_1} + \frac{t_{99}}{Q_{99}} - \left(\frac{tv_1}{Q_1} + \frac{tv_{99}}{Q_{99}} \right)$$

where t_1 , t_2 and t_{99} are travel times through the layers corresponding to the Q model (Q_1 , Q_2 , Q_{99}) to the HRSN stations and tv_1 and tv_{99} are the travel times to V938

through layers Q_1 and Q_{99} respectively. Extra layers can be included by adding t_n/Q_n terms as appropriate.

I observe Δt^* , assume $Q_{99} = 1000$ (P and S) and calculate the travel times, leaving two unknowns, Q_1 and Q_2 (or more if the model is extended). Rearranging equations (3) into matrix form allows me to invert for these unknowns using the inversion routine in MATLAB.

Out of a possible 81 equations (9 earthquakes, 9 stations) some ratios are unusable, either because of clipping or low signal to noise. The number of equations used in each inversion is included in Table 3. I calculate the variance for each inversion, and the formal errors in each Q from the covariance matrix using standard techniques.

6.2 Inversion Results

The preferred model, with a single Q layer on each side of the fault above the fixed high Q layer extending to depth, is shown in figure 6 and the results are given in Table 4. The principal result is that the attenuation on the NE side of the fault is approximately twice that on the SW side for both P and S waves ($Q_2 \sim 2Q_1$). These values represent the average attenuation between the borehole instruments and a depth of 5 km. They do not include the effects of the upper few hundred meters, above the HRSN stations. Using the borehole stations resolves the ambiguity in distributing the attenuation between the very near surface (< 100 m) and deeper layers, which is present in inversions using only surface data [e. g. *Scherbaum*, 1990].

There is little real difference between the inversions using the HRSN and NCSN locations. The NCSN locations are deeper and so have slightly longer travel times and hence higher Q , but this is not significant even within the formal errors. The variances for models using either location or window length are also very similar, approximately 10^{-4} s

for P waves and 3×10^{-4} for S waves. The principal finding that $Q_2 \sim 2Q_1$ is resolved using both sets of locations. The same is true for models in which the velocity structure is varied. The absolute values of Q_1 and Q_2 vary, but the ratio remains stable. Note that using the same velocity structure on both sides of the fault would increase the ratio Q_2 / Q_1 . Essentially, within the uncertainties in velocity and earthquake location, I obtain $Q_2 \sim 2Q_1 \sim 200$ for both P and S waves. If we assume that on average the sedimentary cover is similar, and of comparable thickness ($\sim 1-2$ km) on each side of the fault, then this result implies that the Franciscan rocks on the NE side of the fault are about twice as attenuating as the granitic Salinian basement on the SW side. This result is in good agreement with the spectral modeling (Table 3) and is also consistent with modeling fault zone trapped waves from earthquakes at Parkfield (Li, pers. com., 1998).

The actual relationship between Q_P and Q_S is hard to resolve, given the larger errors in Q_S , and the fact that Q_S / Q_P is directly proportional to α/β . They certainly could be the same, or Q_S could be smaller, or possibly even larger than Q_P . Using a higher α/β as has been suggested around Middle Mountain [e. g. *Eberhart-Phillips and Michael, 1993*] I would increase Q_S / Q_P . S wave attenuation is always higher than P wave attenuation, however, because of the longer travel times.

Figure 7 shows the residuals for the HRSN, 1 s model. They are well distributed, with no difference on either side of the fault. The highest residuals are at station RMN and are in excellent agreement with the relatively shallow depth of this station and the Q values estimated from the spectral modeling (Table 3). The large positive residuals reflect the inclusion of more shallow, low Q material in the path to station RMN than to the other deeper sensors. The residuals at RMN are similar in magnitude to the average attenuation along the paths to the other stations, implying that the attenuation between 63 m and about 250 m depth could be similar to that along the rest of the deeper ray path at Parkfield on the NE side of the fault. Interestingly, the residuals to the deepest HRSN station (VAR, 572 m) are small. They are slightly negative, consistent with Q increasing with depth. The relative residuals at VAR and RMN combine to support a decreasing rate

of increase in Q with depth as has been suggested previously ([. g. Abercrombie, 1997; 12998].

The other station with large (negative) residuals) is GHI. This station is located on the gabbro of Gold Hill [Sims, 1988], which could reasonably be expected to be less attenuating than the sediments beneath the other stations. Also this station is the furthest from Middle Mountain (figure 1), south of the low velocity zone [Eberhart-Phillips and Michael, 1993; Michelini and McEvilly, 1991] and so these residuals could also result from discrepancies between the assumed and actual travel times.

Including additional Q layers on each side of the fault always resulted in an unconstrained inversion, even when either the shallow or deeper layer is assumed to be the same on each side of the fault. The deeper Q to the SW always becomes negative, or infinity if a positivity constraint is included in the inversion. On both sides, however, the inversions clearly prefer Q to increase with depth.

In order to investigate the depth dependence of Q , within the resolution of the data, I try another model with two unknowns. I assume that attenuation does not vary across the fault and inverted for two Q layers above the Q_{99} layer. I vary the relative thicknesses of the two Q layers. These models do not fit the data as well as the models with attenuation differing on each side of the fault. The variances are 50% higher. The shallow layer is always lower Q than the deeper one, consistent with the idea that Q increases with depth. For example, in one model with the upper Q layer extending from the HRSN stations to sea level (approximately 250 to 500 m depth at Parkfield) $Q_P \sim 40$, $Q_S \sim 35$, and in the lower layer, extending to 5 km, $Q_P \sim 100$ and $Q_S \sim 80$. Increasing the depth extent of the shallow layer increases the average Q values, as would be expected.

6.3 Attenuation within the San Andreas Fault Zone

I use the spectral ratios of station MMN to V938 to estimate the attenuation within the San Andreas fault zone. I model the ratios with equation (2) to obtain

$$\Delta t^* = t^*_{MMN} - t^*_{V938}$$

I calculate t^*_{V938} using the inversion results for the preferred model with a single Q on each side of the fault above a high Q half-space (figure 6). Again, I use both HRSN and NCSN locations, and also spectral ratios derived from both window lengths. I use the observed travel times (P time minus origin time for the relevant location) to convert to Q , and then average all the events. I include the results in Table 4. Since no higher Q at depth is included for the fault zone, I exclude the 2 deepest events (3 and 10) from the mean value, and so the Q obtained can be considered an average of the path between MMN and about 5 km depth. The resultant $Q_P \sim 50$ and $Q_S \sim 80$ (Table 4) are in good agreement with the values obtained from the spectral modeling ($Q_P \sim 78$, $Q_S \sim 90$, Table 3).

Again, there is a direct trade off between velocity and Q , as well as between α/β and Q_S/Q_P . Combining the observed travel times with the hypocentral distances for both location sets yields $\alpha \sim 4.8 \pm 0.1$ km/s and $\beta \sim 2.6 \pm 0.3$ km/s. This P wave velocity is very similar to that used on the NE side of the fault, but the S velocity is much lower ($\alpha/\beta \sim 1.8$ -2 within the fault zone). These values are consistent with those from the 3D velocity studies [e. g. *Eberhart-Phillips and Michael*, 1993; *Michellini and McEvilly*, 1991], but the uncertainty in α/β means we cannot conclude that $Q_S > Q_P$ within the fault zone. They do, however, constrain Q within the fault zone to be significantly lower than on either side of the fault.

Previous studies are also consistent with the San Andreas fault being a low Q , low velocity zone. For example, *Blakeslee et al.* [1989] used a spectral ratio method in which pairs of earthquakes recorded at pairs of stations are combined to estimate Q_S of between 26 and 38 at a depth of 5–6 km within the San Andreas fault zone at Parkfield. They assume a higher S wave velocity (3 km/s) than in the present study, and so obtain a lower Q for the same Δt^* . Their result is consistent with that obtained here within the various uncertainties.

Observations seismic waves trapped within major active fault zones have also been used to estimate attenuation and velocity within the zone. At Parkfield, *Li et al.* [1997] uses explosion sources along the fault to estimate $Q_S \sim 30$ within the San Andreas fault zone in the depth range approximately 0–1 km. Using earthquakes as sources Li (pers. comm., 1998) estimated $Q_S \sim 50$ –60 at depths of a few kilometers, in excellent agreement with the results obtained here. The trapped wave studies imply that Q_S increases with depth in the fault zone, as it does in the surrounding rock. An increase in Q_S with depth is also observed within the Landers fault zone (southern California), with absolute values similar to those at Parkfield (*Li et al.* [1994], Li pers. comm., 1998).

6.4 Summary

Inverting the spectral ratios between the HRSN recordings and the deepest Varian seismometers reveals that Q on the SW side of the San Andreas fault in Salinian basement (Q_2) is approximately twice that on the NE side in the Franciscan rocks (Q_1). Between about 250 m and 5 km depth, $Q_2 \sim 2Q_1 \sim 200$ is a reasonable approximation for both P and S waves within the uncertainties in event locations, velocity structure and spectral ratios. Using station MMN, Q within the fault zone is found to be significantly lower than on either side, consistent with earlier indications. The uncertainties in velocity structure mean that the relationship between Q_P and Q_S , both within and on either side of the fault zone, is pretty poorly resolved. They are similar and could be equal within uncertainties.

A number of different observations imply that Q increases rapidly with depth in the upper few kilometers, consistent with the measurements made in the Varian well, and other deep boreholes [*Abercrombie*, 1998]. The large positive residuals to the shallowest station (RMN) suggest that the attenuation between 63 m and about 250 m is similar to the attenuation between 250 m and 5 km depth. The small negative residuals between 250 and 600 m depth (at Varian) are consistent with the rate of increase in Q with depth decreasing with depth. The data are insufficient to constrain fully an inversion with additional depth layers and different Q on each side of the fault, but increasing Q with

depth is clearly preferred. Also, an inversion, in which Q is assumed to vary with depth but not across the fault clearly resolves Q increasing with depth.

7. Site Effects using Surface Recordings

So far, this study has concentrated on attenuation in the crust at depths greater than the borehole seismometers, typically a few hundred meters. Most seismometers, however, are installed at the earth's surface (or in very shallow holes), and of course that is where most people live and structures at risk from earthquakes are built. It is worthwhile, therefore, to investigate the effects of the shallowest layers on the wave propagation. In fact, it is well accepted that the upper 30 m alone has a significant effect on ground shaking out of all proportion to its thickness relative to the total distance traveled by the waves ([Anderson *et al.*, 1996]. Thus, I compare surface and borehole recordings to investigate these shallow effects.

Again, I assume that the difference between a borehole recording and that directly above it represents the effect of the rock in between on the seismic waves. NCSN (surface) seismometers are located close to the wellheads of three of the HRSN boreholes: GHV above GHI at Gold Hill, MMV above MMN at Middle Mountain and VCV above VCA at Vineyard Canyon (figure 1). Stations HPV and PCV are located within 3 km of station SMN and so I also compare these stations to SMN, although the horizontal offsets decrease the validity of the underlying assumptions. I also compare recordings made at the surface and 23 m depth in the Varian Well with those at 298 and 572 m.

The mean ratios between the surface and borehole recordings at Gold Hill, Middle Mountain and Vineyard Canyon are shown in figure 7. Note that for such shallow boreholes, both windows used include the surface reflection. The frequency bandwidth is limited by the lower sampling rate of the NCSN, and also by the higher noise at the surface sites. No S waves were well recorded at both downhole and surface stations at Gold Hill and Vineyard Canyon from the 9 earthquakes. Essentially all the ratios show

amplification of between 3 and 6 times over the entire frequency range of 3 to about 30 Hz. The ratios between HPV and PCV and SMN are very similar to those shown in figure 7. The amplification includes the free surface effect, and so the actual amplification is about 1.5 to 3 times, consistent with measurements at other hard rock and sedimentary sites (reference, 19??).

It is interesting that no attenuation is observed in these ratios. This is probably because at these frequencies, the distance between the stations is such a small number of wavelengths that even a very low Q would have little effect (e. g. at 1 km/s, 3 - 30 Hz corresponds to wavelengths of 300 - 30 m). *Blakeslee and Malin* [1991] installed two surface seismometers at the wellheads of JCN and VCA to investigate the near surface effects. They used a higher sample rate at the surface than NCSN and obtained ratios over a greater bandwidth, up to 100 Hz for P waves. My results are in good agreement with theirs for Vineyard Canyon below about 30 Hz, where their spectral ratios are dominated by amplification of about a factor of four. At higher frequencies, however, their spectral ratios clearly show strong attenuation, and they calculate Q to be about 10 in the upper 200 m at these sites.

To investigate site effects at the Varian Well, I calculate spectral ratios between 0 and 298 m, 0 and 572 m, and 23 and 298 m (no data are available for both 23 and 572 m), figure 8. These ratios demonstrate well the competing effects of amplification and attenuation in the very near surface. Both effects are frequency and depth dependent.

For both P and S waves, at low frequencies (below about 8 Hz) near surface amplification dominates all three ratios. They are all very similar, suggesting that these wavelengths are not greatly affected by either the upper 20 m nor the 300 - 600 m depth range, but perhaps by the entire 0-600 m range. At higher frequencies, the 0/298 m ratios remain relatively constant, dominated by amplification. The 0/572 m ratios fall off rapidly at higher frequencies implying that attenuation in the upper 600 m exceeds the near surface amplification for these frequencies. The 23/298 m ratios also decrease with frequency at

high frequencies, although less than the 0/572 m ratios. I interpret this as implying that the total attenuation between 23 and 298 m is less than between 0 and 600 m, and that the amplification of frequencies higher than about 8 Hz is concentrated in the very shallow layers (sampled here at 20 m). The absolute amplification at a site is of course dependent on the entire ray path. If high attenuation exists at greater depths, then even large amplification of high frequency energy in the upper 30 m or so will not produce strong shaking. For example, sites on either side of the San Andreas fault at Parkfield with identical site effects in the upper 30 m would not experience similar shaking because of the large difference in attenuation at greater depth. The results of this study therefore confirm the numerical simulations of *Anderson et al.* [1996]. They found that although the upper 30 m, typically used to evaluate site effects, has a large effect on the recorded ground motions, the attenuation beneath this depth, extending to perhaps a few kilometers, can effect the recorded amplitudes by a comparable amount.

8. Conclusions

In this study, I combine earthquake recordings at a borehole network of 10 stations (averaging about 250 m deep), at 7 depths in the Varian well (0–938 m depth) and at the surface. I use these records, and a number of spectral techniques, to measure attenuation as a function of depth in the upper crust, on each side of the San Andreas fault, and within the fault zone itself. The principal conclusions are:

1. Attenuation to the NE of the San Andreas fault at Parkfield is approximately twice that to the SW. $Q_{SW} \sim 2Q_{NE} \sim 200$ between about 200 and 5000 m depth. Q_P and Q_S are similar, but their ratio is not well resolved.
2. The San Andreas fault is confirmed to be a strongly attenuating zone with $Q_P \sim 50$ and $Q_S \sim 80$. Again, the ratio of Q_P to Q_S is not well resolved.
3. Q increases with depth, with the rate of increase most rapid at shallow depths (less than a few hundred meters). For example, comparison of recordings at different

depths in the Varian Well yields $Q_P \sim 30$ and $Q_S \sim 20$ in the upper 1 km, with Q_P increasing from about 20 between 0 and 300 m to about 55 between 600 and 1000 m.

4. None of the instrumented boreholes in the Parkfield area are deep enough for attenuation to be considered negligible in analyses of small earthquake sources. The attenuation to the deepest (1 km) instrument) on the NE side of the fault is comparable to that below instruments at only about 200 m on the SW side.
5. Amplification of about a factor of 3 – 6 (including the free surface effect) is observed in the upper few hundred meters. The results of this study imply that both the amplification in the very shallow layers (surficial geology, <30 m) and the amplification and attenuation at greater depths (up to a few km) are equally important in estimating the site effects for seismic hazard studies.

Acknowledgments. I am grateful to P. Malin, R. Nadeau, P. Johnson, D. Oppenheimer and the Northern California Data Center for providing data and assistance with reading it. R. Nadeau, P. Malin, P. Johnson and M. Antolik provided useful background information about the Parkfield area and instrumentation. Discussions with R. Benites, and J. Taber were also fruitful. Reviews by .. This work was funded by NEHRP award NC5135 to the University of Southern California, and I also received support from IGNS, New Zealand, and Harvard University.

References

- Abercrombie, R. E., Near surface attenuation and site effects from comparison of surface and deep borehole recordings, *Bull. Seismol. Soc. Am.*, **87**, 731-744, 1997.
- Abercrombie, R. E., The magnitude-frequency distribution of earthquakes recorded with deep seismometers at Cajon Pass, southern California, *Tectonophys.*, **261**, 1-7, 1996.
- Abercrombie, R. E., Earthquake source scaling relationships from -1 to 5 M_L using seismograms recorded at 2.5 km depth, *J. Geophys. Res.*, **100**, 24015-24036, 1995.
- Abercrombie, R. E. and P. Leary, Source parameters of small earthquakes recorded at 2.5 km depth, Cajon Pass, southern California: implications for earthquake scaling, *Geophys. Res. Letts.*, **20**, 1511-1514, 1993.
- Adams, D. A. and Abercrombie, R. E., Seismic attenuation at high frequencies in southern California from coda waves recorded at a range of depths. *J. Geophys. Res.*, **103**, 24257-24270, 1998.

- Anderson, J. G., Y. Lee, Y. Zeng and S. Day, Control of strong ground motion by the upper 30 meters, *Bull. Seismol. Soc. Am.*, 86, 1749-1759, 1996.
- Anderson, J. G. and S. E. Hough, A model for the shape of the Fourier amplitude spectrum of acceleration at high frequencies, *Bull. Seismol. Soc. Am.*, 74, 1969-1993, 1984.
- Archuleta, R. J., E. Cranswick, C. Mueller and P. Spudich, Source parameters of the 1980 Mammoth Lakes, California, earthquake sequence, *J. Geophys. Res.*, 87, 4595-4607, 1982.
- Aster, R. C. and P. M. Shearer, High-frequency borehole seismograms recorded in the San Jacinto fault zone, southern California, part 2. attenuation and site effects, *Bull. Seismol. Soc. Am.*, 81, 1081-1100, 1991.
- Ben-Zion, Y. and P. E. Malin, San Andreas fault zone head waves near Parkfield, California, *Science*, 251, 1592-1594, 1991.
- Blakeslee S. and P. Malin, High-frequency site effects at two Parkfield downhole and surface stations, *Bull. Seismol. Soc. Am.*, 81, 332-345, 1991.
- Blakeslee, S., P. Malin and M. Alvarez, Fault-zone attenuation of high-frequency seismic waves, *Geophys. Res. Lett.*, 16, 1321-1324, 1989.
- Boatwright, J., A spectral theory for circular seismic sources: simple estimates of source dimension, dynamic stress drop and radiated energy, *Bull. Seismol. Soc. Am.*, 70, 1-27, 1980.
- Boatwright, J., Regional propagation characteristics and source parameters of earthquakes in northeastern North America, *Bull. Seismol. Soc. Am.*, 84, 1-15, 1994.
- Brune, J.N., Tectonic stress and the spectra of seismic shear waves from earthquakes, *J. Geophys. Res.*, 75, 4997-5009, 1970.
- Celebi, M., J. Prince, C. Dietal, M. Onate and G. Chavez, The culprit in Mexico City - amplification of motions, *Earthq. Spectra*, 3, 315-328, 1987.
- Clawson et al..
- Eberhart-Phillips, D. and A. Michael, Three-dimensional velocity structure, seismicity and fault structure in the Parkfield region, central California, *J. Geophys. Res.*, 98, 15737-15758, 1993.
- Eshelby, J. D., The determination of the elastic field of an ellipsoidal inclusion and related problems, *Proc. R. Soc. London A*, 241, 376-396, 1957.
- Hauksson, E., T-L. Teng and T. L. Henyey, Results from a 1500 m deep, three-level downhole seismometer array: site response, low Q values and f_{max} , *Bull. Seismol. Soc. Am.*, 77, 1883-1904, 1987.
- Hough, S. E., J. G. Anderson, J. Brune, F. Vernon, J. Berger, J. Fletcher, L. Haar, T. Hanks, and L. Baker, Attenuation near Anza, California, *Bull. Seismol. Soc. Am.*, 78, 672-691, 1988.
- Johnson, P. A. and T. V. McEvilly, Parkfield seismicity: fluid driven?, *J. Geophys. Res.*, 100, 12937-12950, 1995.
- Jongmans, D. and P. E. Malin, Vertical profiling of microearthquake S waves in the Varian well at Parkfield, California, *Bull. Seismol. Soc. Am.*, 85, 1805-1820, 1995.

- Karageorgi, E., R. Clymer and T. V. McEvilly, Seismological Studies at Parkfield II, Search for temporal variations in wave propagation using Vibroseis, *Bull. Seismol. Soc. Am.*, 82, 1388-1415, 1992.
- Lee and Lahr, HYPO71
- Li, Y-G., W. L. Ellsworth, C. H. Thurber, P. E. Malin and K. Aki, Fault zone guided waves from explosions in the San Andreas fault at Parkfield and Cienega valley, California, *Bull. Seismol. Soc. Am.*, 87, 210-221, 1997.
- Li, Y-G., K. Aki, D. Adams, A. Hasemi and W. H. K. Lee, Seismic guided waves trapped in the fault zone of the Landers, California, earthquake of 1992, *J. Geophys. Res.*, 99, 11705-11722, 1994.
- Li, Y-G., P. C. Leary, K. Aki and P. E. Malin, Seismic trapped modes in the San Andreas fault zones, *Science*, 249, 763-766, 1990.
- Madariaga, R., Dynamics of an expanding circular fault, *Bull. Seismol. Soc. Am.*, 66, 639-666, 1976.
- Malin, P. E., Blakeslee, S. N., Alvarez, M. G. and Martin, A.J., Microearthquake imaging of the Parkfield asperity, *Science.*, 244, 557-559, 1989.
- Malin et al. 1987.
- Micheline, A. and T. V. McEvilly, Seismological Studies at Parkfield I: Simultaneous inversion for velocity structure and hypocenters using B-splines parameterization, *Bull. Seismol. Soc. Am.*, 81, 524-552, 1991.
- Nadeau, R. M. and T. V. McEvilly, Seismological Studies at Parkfield V: characteristic microearthquake sequences as fault-zone drilling targets, *Bull. Seismol. Soc. Am.*, 87, 1463-1472, 1997.
- Nadeau, R. M., M. Antolik, P. A Johnson, W. Foxall and T. V. McEvilly, Seismological Studies at Parkfield III: microearthquake clusters in the study of fault zone dynamics, *Bull. Seismol. Soc. Am.*, 84, 247-263, 1994.
- Page, B. M., The Southern Coastal Ranges, in *The Geotectonic Development of California, Rubey Vol. I*, edited by W. G. Ernst, pp329-417, Prentice-Hall, Englewood Cliffs, H. J., 1981
- Sanders, C. O., Local earthquake tomography: attenuation - theory and results, in *Seismic Tomography: Theory and Practice*, edited by H. M. Iyer and K. Hirahara, pp?-? Chapman and Hall, London, 1993.
- Scherbaum, F., Combined inversion for the three-dimensional Q structure and source parameters using micro-earthquake spectra, *J. Geophys. Res.*, 95, 12423-12438, 1990.
- Sims, J. D., Geologic Map of the San Andreas fault in the Cholame Valley and Cholame Hills quadrangles, Monterey and San Louis Obispo counties, California, scale 1:24,000, *U. S. Geol. Surv. Misc. Field Stud. Map, MF-1995*, 1988.
- Sims, J. D., Geologic Map of the San Andreas fault in the Parkfield 7.5-minute quadrangle, Monterey and Fresno counties, California, scale 1:24,000, *U. S. Geol. Surv. Misc. Field Stud. Map, MF-2115*, 1990.

Table 1. Hypocentral Parameters

N	Date and Time	NCSN Location				HRSN Location				M_L
		Sec.	Lat (°)	Long (°)	Depth (km)	Sec.	Lat (°)	Long (°)	Depth (km)	
3	89/01/29/15:33	41.43	35.9810	120.5267	11.14	-	-	-	-	1.3
5	89/08/02/07:42	58.82	35.9280	120.4760	4.67	58.82	35.9238	120.4815	3.3	1.1
6	89/08/06/21/:00	34.52	36.0047	120.5607	5.31	34.69	36.0003	120.5694	2.9	2.1
7	89/08/07/03:54	50.98	36.0020	120.5612	5.13	50.99	36.0047	120.5729	3.7	2.1
8	89/08/08/01:19	7.03	35.9263	120.4800	4.41	7.15	35.9233	120.4811	3.3	1.0
9	90/01/25/02:26	53.44	36.0240	120.5727	5.41	-	36.0237	120.5938	4.4	1.4
10	90/01/25/08:38	16.20	35.9595	120.5032	11.33	16.43	35.9453	120.5264	10.2	1.7
11	90/01/31/10:33	1.97	35.9232	120.4692	5.01	2.17	35.9190	120.4768	3.7	1.1
12	90/01/31/10:52	43.03	35.9230	120.4690	5.14	43.24	35.9190	120.4763	3.7	1.1

N is the Event Number (same as that used by *Jongmans and Malin*, 1995).
Date and time are given as Year/Month/Day/Hour:minute.
Events 3 and 9 were not located by the HRSN. Event 9 is identified as a member of a well located cluster and so that location is given (R. Nadeau, pers. comm., 1998).
Longitude is in degrees west.

Table 2. Source Parameters from Spectral Modeling including attenuation

Event	M_0	Radius	$\Delta\sigma$
	($\times 10^{12}$ Nm)		
3	0.48	41	4.5
5	0.29	45	1.3
6	8.27	84	7.0
7	2.14	48	8.0
8	0.25	50	0.9
9	0.86	50	4.7
10	1.22	35	12.6
11	0.25	39	1.9
12	0.33	47	1.3

Table 3. Q Values from Spectral Modeling

Station	Q_P	Error Q_P	Q_S	Error Q_S	Sensor Depth (m)
SMN	373	296	255	84	282
VCA	159	59	131	0	200
FRO	170	34	130	0	284
MMN	78	16	90	29	221
RMN	57	8	70	10	73
JCN	126	25	159	16	224
VAR	147	24	136	49	572
EAD	118	33	173	43	245
V938	182	29	149	25	938
SW	201	71	205	75	200-284
NE	128	18	159	25	224-572

The errors are the 95% confidence limits.
SW is the mean of stations SMN, VCA and FRO, and NE is the mean of stations JCN, VAR and EAD. The depth range of the sensors is given in each case. Station JCS is at 176 m depth, and GHI is at 145 m.

Table 4. Q Values above 5 km from Inversion

Location	HRSN (1s)				NCSN (1s)			
	Q_P	N_P	Q_S	N_S	Q_P	N_P	Q_S	N_S
NE	139	54	98	42	99	61	84	48
	(133-147)		(92-118)		(95-109)		(80-102)	
SW	246	54	268	42	199	61	236	48
	(224-305)		(223-408)		(179-242)		(197-316)	
SAF	52	6	78	6	49	7	78	7
	(35-69)		(49-107)		(35-63)		(50-106)	

NE is the north-east side of the San Andreas fault, SW the south-west and SAF is the fault zone, from station MMN. N_P and N_S are the number of P and S spectral ratios, respectively, used in the inversion. The 95% confidence interval is given in parentheses.

Figure Captions

Figure 1. Parkfield location map showing the HRSN stations (solid triangles) and the NCSN stations (inverted triangles) used in this study. Station VAR is the location of the Varian Array. All three locations for each earthquake are shown: the NCSN (diamonds), the Duke University (squares) and the HRSN (circles). The surface trace of the major faults are marked - the San Andreas Fault runs through Middle Mountain (stations MMN and MMV) and the town of Parkfield (star).

Figure 2. Velocity seismograms for event 12. They are raw velocity seismograms, aligned on the P wave arrival. At each station the top trace is the vertical, the middle the NS horizontal and the bottom trace is the EW horizontal. The horizontal orientations are approximate for V938 – see *Jongmans and Malin* [1995] for exact orientation of the sensor. Note that the waveforms at VCA (on the SW side of the fault) are less attenuated and scattered than those recorded at JCN (on the NE side) and MMN (within the fault zone). The waveforms at V938 look most similar to those at VCA.

Figure 3. P and S wave spectra from 1 second windows for the same event at the same stations as figure 2. The solid lines are the signal spectra, the dotted are the noise, and the dashed lines are the fits using equation 1.

Figure 4. Moment and source dimension. The dashed lines are of constant stress drop.

Figure 5. Spectral ratios of various depth recordings of event 5 at the Varian array. They are fairly linear on the log-linear plots, and the gradients decrease as the depth interval becomes smaller and deeper. All plots are at the same scale. The dashed lines are the fits using equation (2).

Figure 6. Q inversion results. (a) shows Q_P (with 95% confidence limits) between the borehole stations and 5 km on each side of the fault, and within the fault zone for the inversion using HRSN locations and 1 s time windows. (b) shows the same for

Q_S . (c) is a cross section perpendicular to the San Andreas fault, showing the layout of the velocity and Q model used in the preferred inversion. The central white column represents the San Andreas fault, and the thick vertical line is the depth range of the earthquakes used. The horizontal solid line is at sea level, and the dashed line approximates the ground surface. The dots represent the sensor depths - the HRSN stations are at about 250 m depth and V938 is at 938 m. The assumed velocity structure on each side of the fault used to calculate the travel times is shown. In this model, Q_1 is the attenuation quality factor between the HRSN sensors and 5 km depth on the NE side of the fault, and Q_2 is that for the same depth range on the SW side of the fault. Q_{99} is assumed to be 1000 on both sides of the fault. Q_{SAF} is the quality factor within the fault zone calculated using station MMN (see text).

Figure 7. Station residuals ($t_{\text{obs}} - t_{\text{pred}}$) for P and S waves from the preferred model.

Squares are used for stations on the SW side of the fault and circles for stations on the NE. The vertical line divides the two sets. For clarity, solid and open symbols are used for alternate stations.

Figure 8. Mean spectral ratios between the surface NCSN and borehole HRSN stations at Gold Hill (GH), Middle Mountain (MM) and Vineyard Canyon (VC). The thick lines are the mean values from all the earthquakes, and the thin lines are at 1 standard deviation.

Figure 9. Mean spectral ratios for all earthquakes at the Varian Well between 0 and 298 m (solid black line), 0 and 572 m (dotted white line) and 23 and 298 m (dashed black line). The mid gray, dark gray and pale gray shaded areas represent 1 standard deviation about the three ratios, respectively.

Map of Parkfield - Earthquakes and Stations

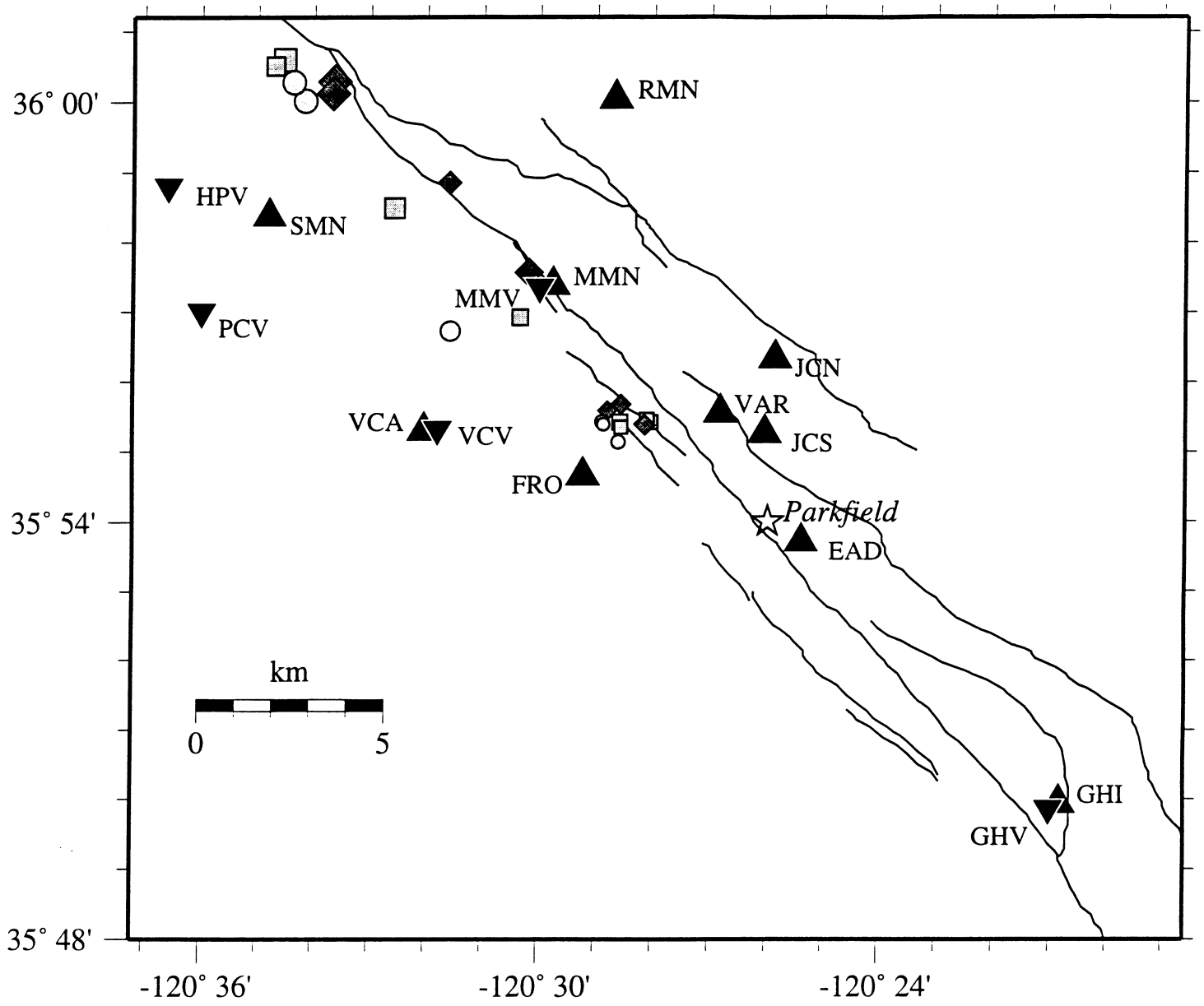


Figure 1

Fig1-map.ps

Figure 2

Event 12 – Raw data aligned on P wave

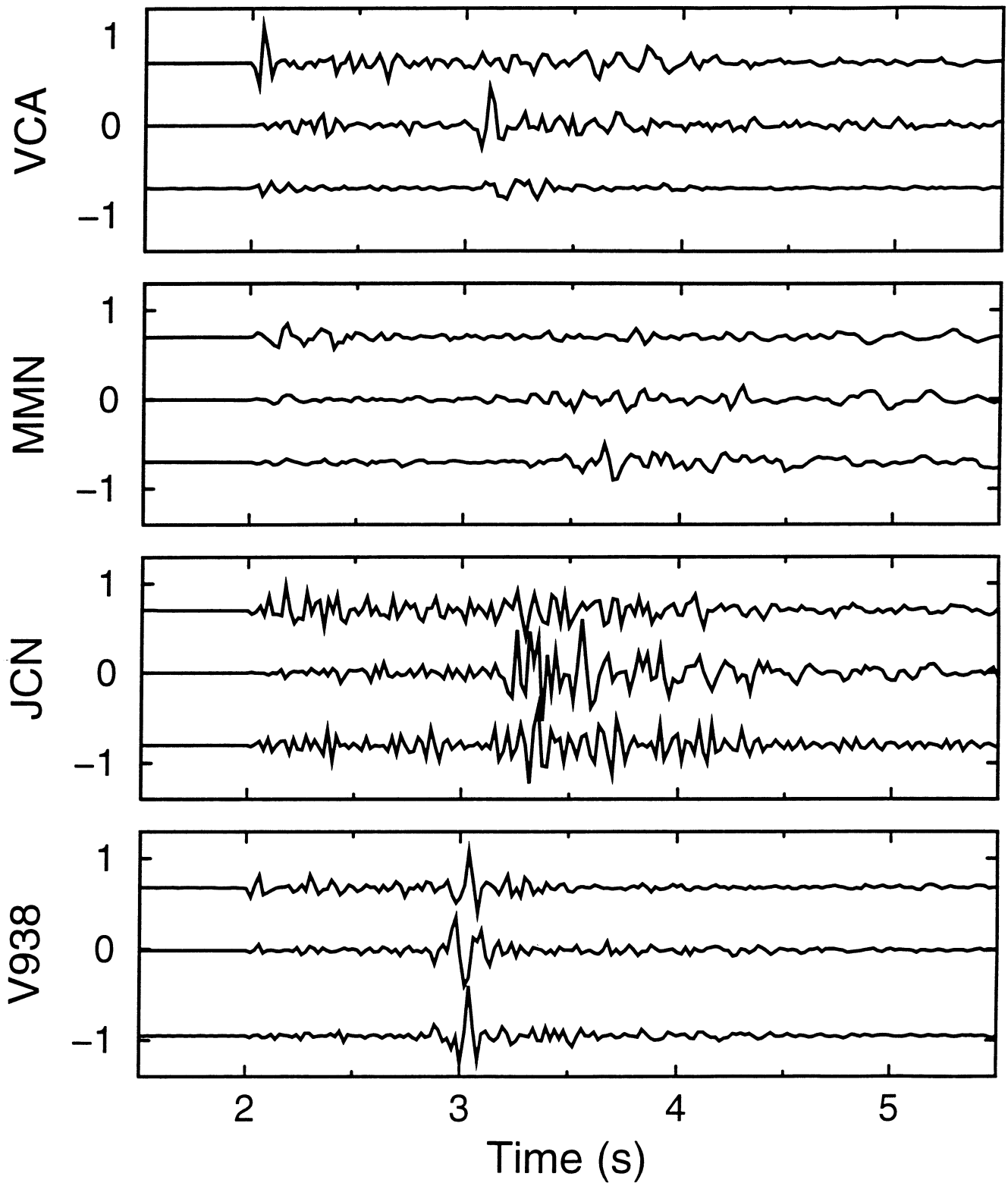


Figure 3

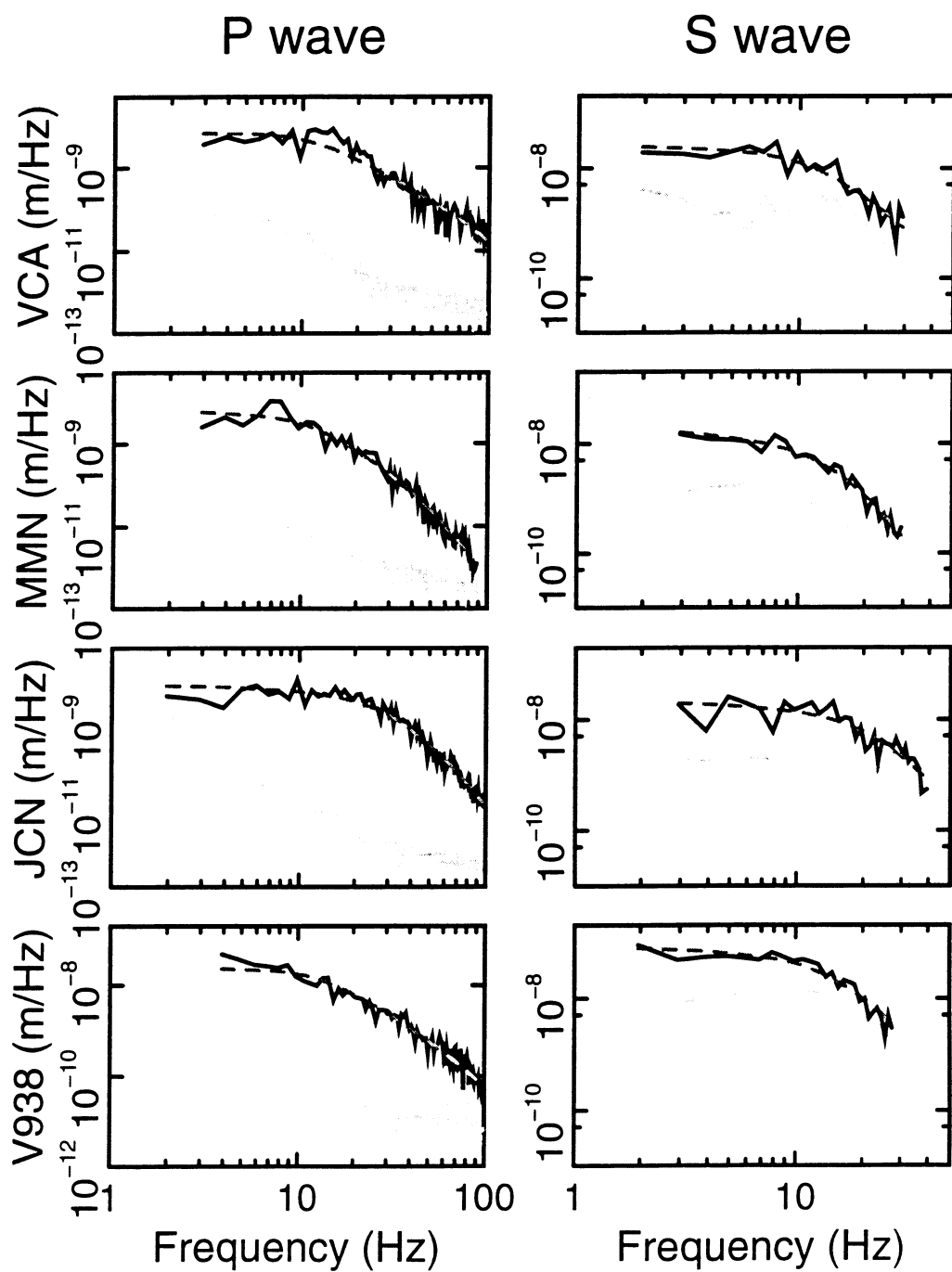


Figure 4.

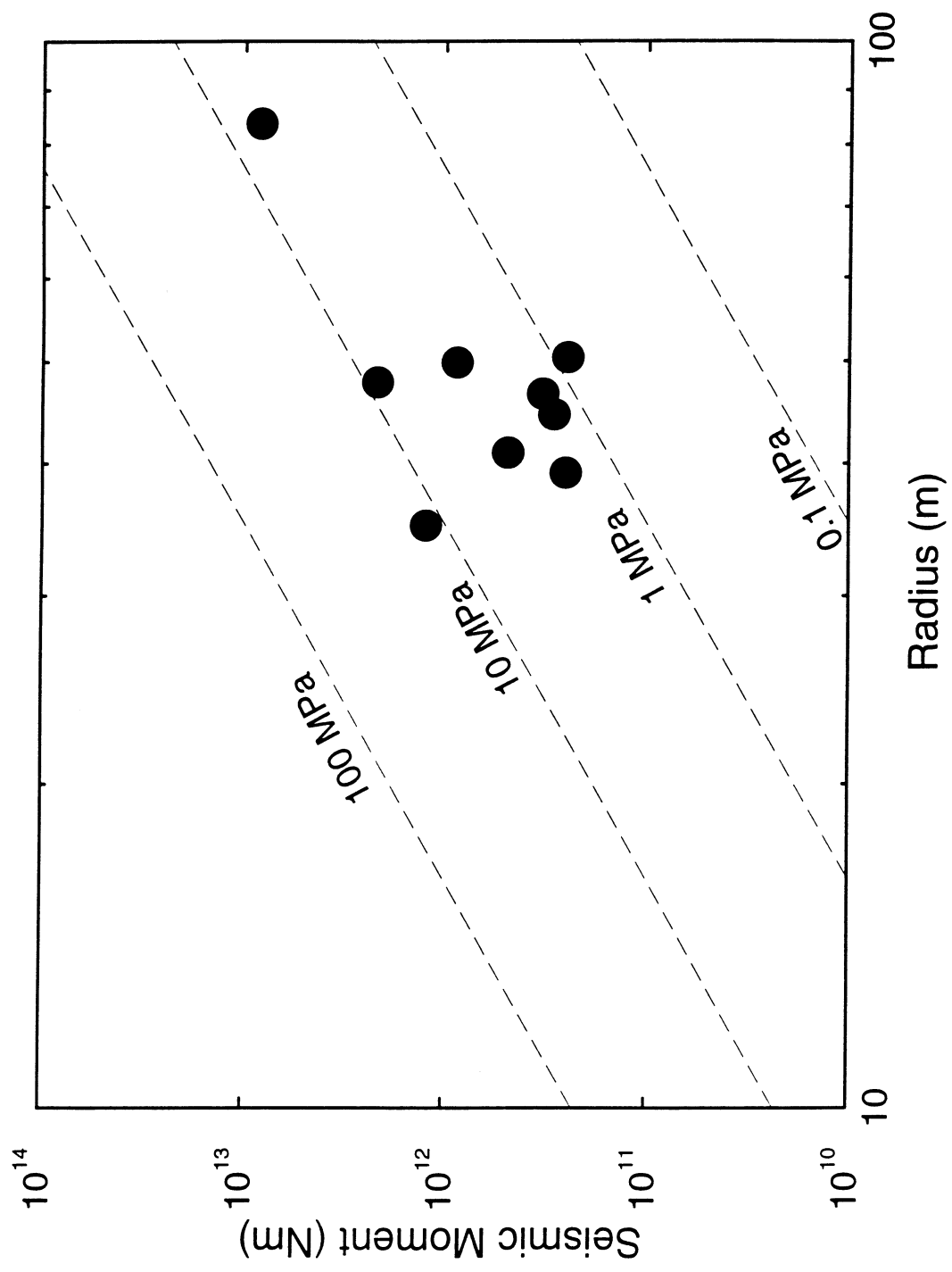


Figure 5

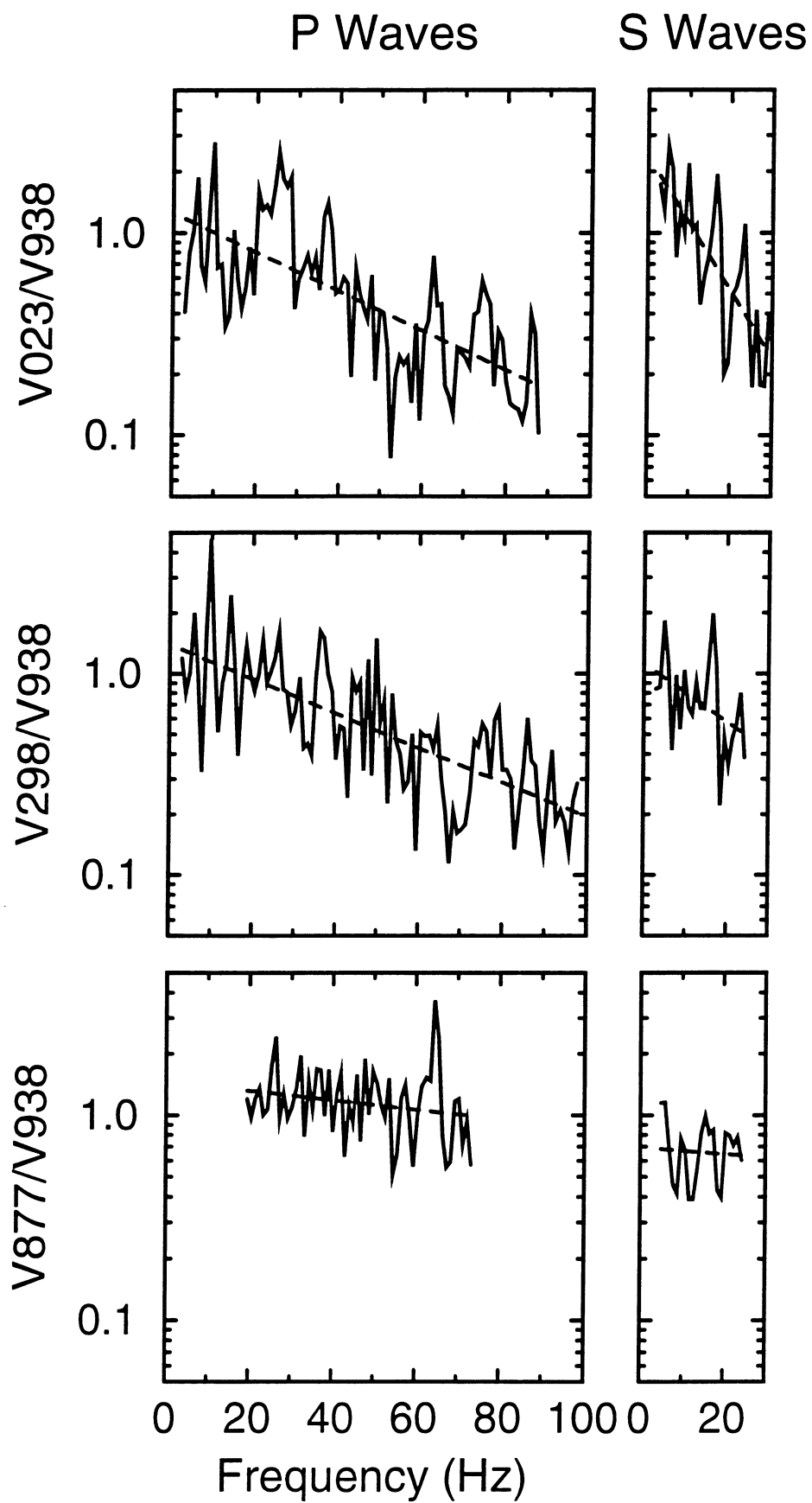


Figure 6

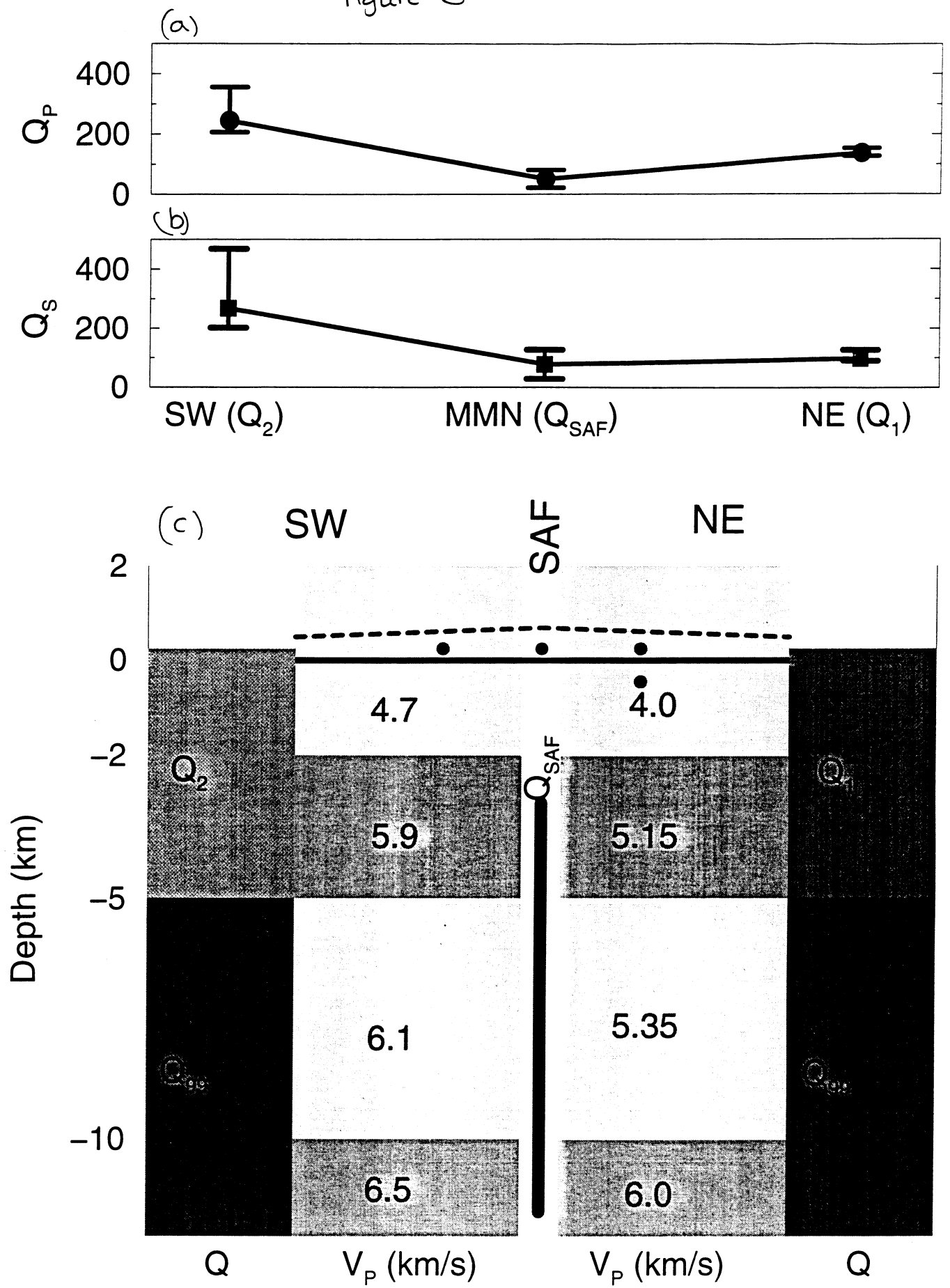
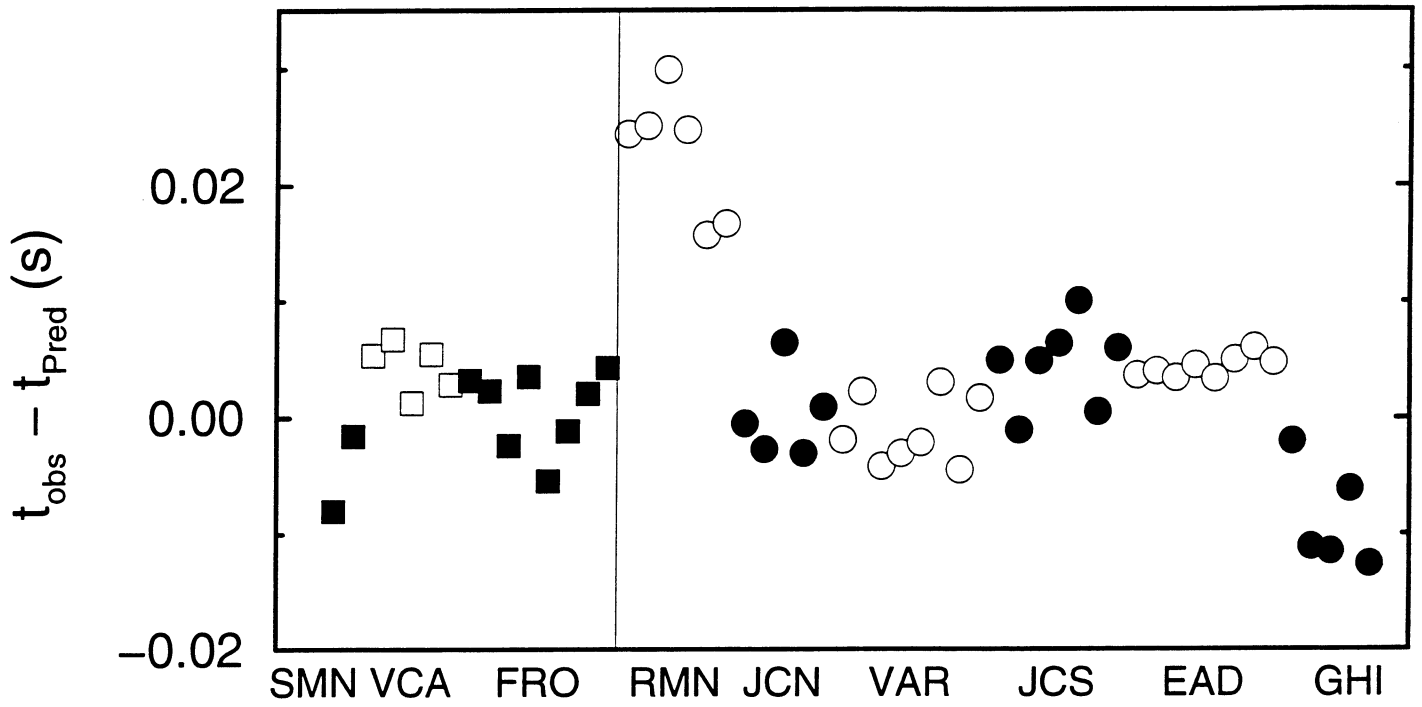


Figure 7

P wave Residuals



S wave Residuals

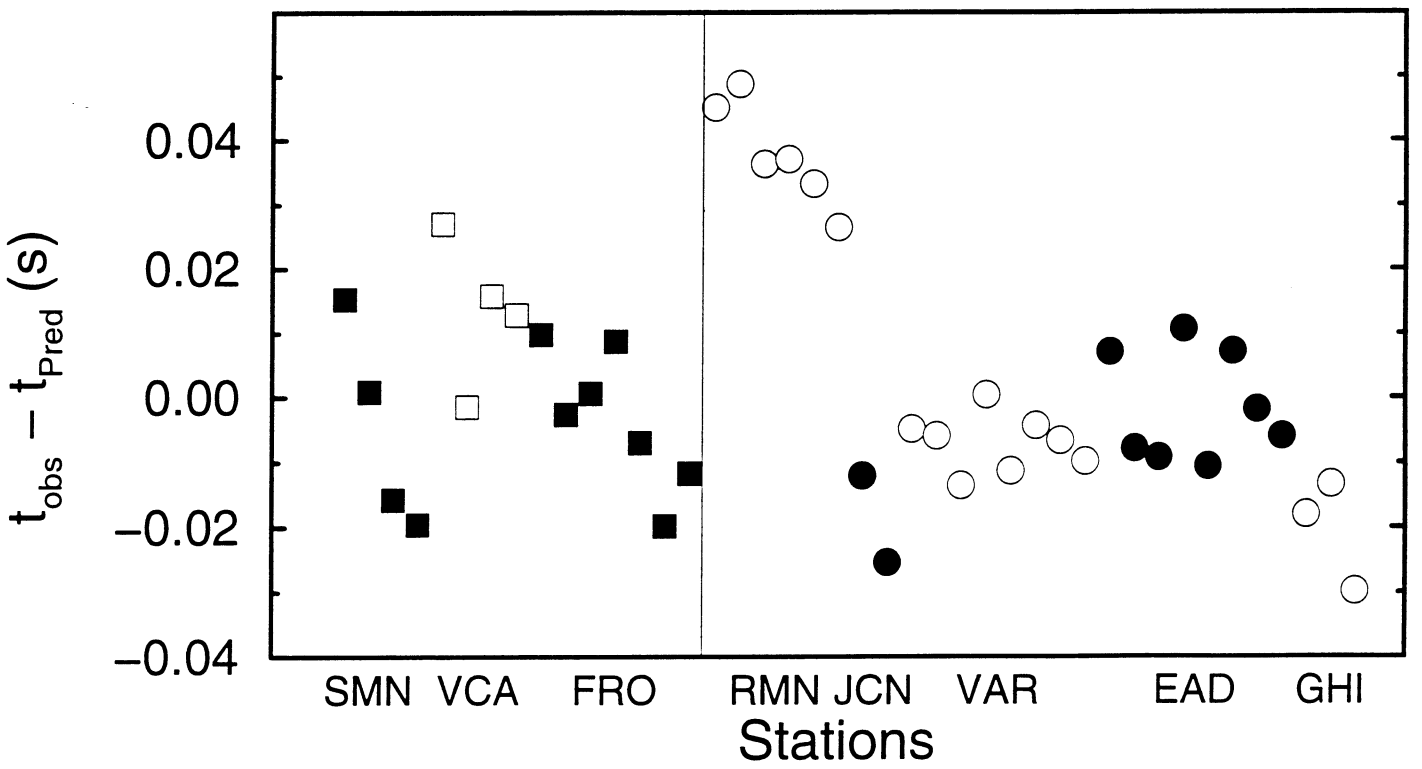


Figure 8

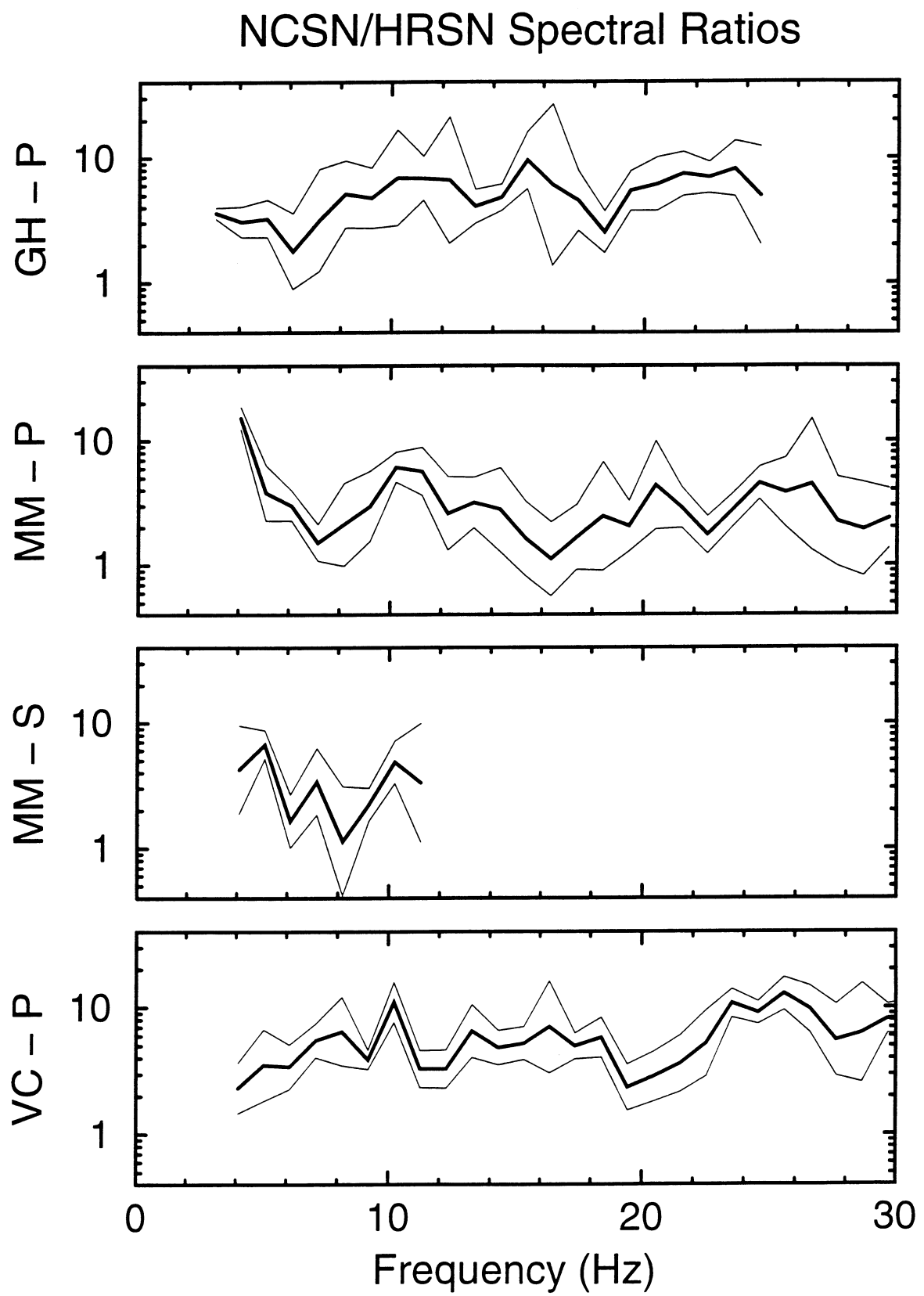


Figure 9

